Solid State Communications 267 (2017) 48–52

Contents lists available at ScienceDirect

Solid State Communications

journal homepage: www.elsevier.com/locate/ssc

Communication

Magnetic fluctuations in $BaFe_{2-x}Ni_xAs_2$ superconductors

M. Saint-Paul[a,b,*], C. Guttin[a,b], A. Abbassi[c], Zhao-Sheng Wang[a,b,d,1], Huiqian Luo[d], Xingye Lu[d], Cong Ren[d], Hai-Hu Wen[d,e], K. Hasselbach[a,b]

[a] Université Grenoble Alpes, Institut Néel, F-38042 Grenoble, France
[b] CNRS, Institut Néel, F-38042 Grenoble, France
[c] Faculté des Sciences et Techniques de Tanger, Université Abdelmalek Essaâdi, BP 416 Tanger, Morocco
[d] Beijing National Laboratory for Condensed Matter Physics, Institute of Physics, Chinese Academic of Sciences, Beijing 100190, China
[e] National Laboratory for Solid State Microstuctures, Departement of Physics, Nanjing University, 210093 Nanjing, China

ARTICLE INFO

Communicated by A.K. Sood

Keywords:
A. Pnictides
D. Superconductivity
E. Surface impedance
Ultrasonic attenuation

ABSTRACT

Anomalies found in the electronic conductivity and the elastic constants C_{33} and C_{44} around the superconducting phase transition in the underdoped $BaFe_{1.93}Ni_{0.07}As_2$ compounds are re-examined. The large anomalies in the elastic constants C_{33} and C_{44} modes and the unusual temperature dependence of the real part σ_1 of the electronic conductivity found around the superconducting phase transition $T_C \sim 16$ K are attributed to magnetic fluctuations. The establishment of a magnetic order at $T_M \sim 21$ K results in a marked decrease of the scattering of electronic carriers.

1. Introduction

The structural and magnetic phases of iron pnictide superconductors $BaFe_{2-x}Ni_xAs_2$ and $BaFe_{2-x}Co_xAs_2$ have been intensively studied [1–19]. Iron based superconductors are very useful in studying the interplay between magnetism and superconductivity. The values of the relevant temperature scales associated (T_N for antiferromagnetic transition and T_C for superconducting transition) vary significantly. In the undoped $BaFe_2As_2$ an antiferromagnetic order $T_N \sim 140$ K coexists with an orthorhombic structural transition $T_S \sim 140$ K. With increasing the electron doping in $BaFe_{2-x}Ni_xAs_2$ and $BaFe_{2-x}Co_xAs_2$ to induce superconductivity, their Néel temperature T_N decreases. The underdoped $BaFe_{1.93}Ni_{0.07}As_2$ exhibits a structural phase transition at $T_S \sim 70$ K, an antiferromagnetic transition at $T_N \sim 50$ K and a superconducting transition at $T_C = 16$ K [8]. Near optimal superconductivity inhomogeneous frozen antiferromagnetic domains have been observed by NMR [6–8] and neutron [4,5] experiments. NMR experiments provide evidence for the existence of magnetic fluctuations competing with superconductivity in the Co and Ni doped $BaFe_2As2$ families. The spin-lattice relaxation rate shows a critical slowing down around T_N and a further strong decrease around the superconducting transition [8].

Metallic or superconducting antiferromagnets affer give the possibility to study the influence of local moments on electronic properties [20]. Effects on the electronic conductivity are expected in the metallic state. In the superconducting state, magnetism can induce effects on the superconducting order parameter [20]. Surface impedance measurements have been published on iron based superconductors (crystals) and they give information on London penetration depth [14–17,19]. The London penetration depth λ_L in the ab plane exhibits a power law behavior approaching T^2 variation in iron based superconductors [15,17,19]. The enhancement of the real part of the conductivity below T_C was explained by a rapid decrease of the quasiparticle scattering [14,15,19]. No clear coherence peak was observed in crystals with microwave measurements [14,15,19].

Elastic constants provide information on magnetic and structural fluctuations [2]. The giant softening of the shear elastic constant C_{66} in the ab plane indicates that structural fluctuations play an important role in the emergence of superconductivity [2]. Furthermore the velocity and attenuation of the longitudinal elastic mode C_{33} and the shear mode C_{44} propagating along the c axis perpendicular to the basal plane show an anomalous behavior around the superconducting phase transition [10,13]. The properties of C_{33} appearing at T_C in Co doped $BaFe_2As_2$ crystals have been related to the magnetic character of these materials in [10]. The presence of magnetic fluctuations in $BaFe_{2-x}Ni_xAs_2$ have been detected by specific heat measurements [3].

We re-analyze our surface impedance results obtained in the underdoped $BaFe_{1.93}Ni_{0.07}As_2$ superconductors and previously published in [12]. Anomalies in the electromagnetic properties [12] and the elastic constants C_{33} and C_{44} [13] found around the superconduct-

* Corresponding author at: Université Grenoble Alpes, Institut Néel, F-38042 Grenoble, France.
E-mail address: Michel.saint-paul@neel.cnrs.fr (M. Saint-Paul).
[1] Present address: High Magnetic Field Laboratory, Chinese Academy of Science Hefei Anhui 230031 China.

http://dx.doi.org/10.1016/j.ssc.2017.08.021
Received 10 May 2017; Received in revised form 29 August 2017; Accepted 31 August 2017
Available online 01 September 2017

ing phase transition in the underdoped $BaFe_{1.93}Ni_{0.07}As_2$ compounds are re-examined. For this study we use our existing data reported in [12,13].

2. Surface impedance measurements

The real σ_1 and imaginary σ_2 parts of the electronic conductivity have been measured in the microwave and millimeter wavelength range in Co [14,15], Ni [16] and K [15,19] doped $BaFe_2As_2$ crystals. The surface impedance results obtained with underdoped $BaFe_{1.93}Ni_{0.07}As_2$ published in [12] are re-examined. Radiofrequency magnetic field is applied parallel to the ab plane. Screening currents both flow in the ab plane and along the c axis. Since the thickness of the samples along the c axis is small, its contribution to the surface impedance is small in comparison with the contribution given by the ab plane. The platelets samples are placed inside a small copper coil. Non resonant measurements of the impedance of the coil were performed with automated impedance analyzer Agilent 4395 in the frequency range 1–100 MHz. Resonant measurements were performed at 1.5 GHz with a Hewlet Packard 8720B network analyzer. The experimental procedure is described in [11,12].

At radiofrequencies (10 MHz to 1 GHz) measurements of the temperature dependence of the surface impedance Z = R+jX yield the temperature dependence of the complex conductivity $\sigma_1 - j\sigma_2$ in the superconducting state.

The real part of the conductivity σ_1 represents the loss related to the conductivity of the normal carriers and quasiparticles (14, 21). The imaginary part of the conductivity σ_2 is related to the London penetration depth λ_L by $\sigma_2 = 1/(\mu_0\omega\lambda_L^2)$ [14], ω is the angular frequency

$$\frac{\sigma_2}{\sigma_2(0)} = \frac{\lambda_L(0)^2}{\lambda_L(T)^2} \quad \frac{\sigma_2}{\sigma_2(0)} \approx 1 - \left(\frac{T}{T_C}\right)^2 \tag{1}$$

where $\sigma_2(0) = \sigma_2(T = 0)$. The quadratic dependence of Eq. (1) works moderately [15,17].

Surface impedance Z = R+jX is given by

$$Z = R + jX = \sqrt{\frac{j\mu_0\omega}{\sigma_1 - j\sigma_2}} \tag{2}$$

where μ_0 is the magnetic permeability of vacuum and ω the angular frequency. Our resistance measurements are well resolved at $T > T_C$ [12]. But at $T < 0.9T_C$ our experimental resolution in the low frequency range (< 100 MHz) is not sufficient to extract the intrinsic resistance and conductivity σ_1. The measurements of X(T) and R(T) are normalized to the values X(25) and R(25) measured at 25 K. The real σ_1 and imaginary σ_2 parts of the conductivity are normalized to the value of the normal conductivity $\sigma(25)$ at 25 K in the normal state. $\sigma(25) = 1/\rho_{dc}$ is the conductivity at 25 K and $\rho_{dc} \sim 10^{-6}\ \Omega$ m is the dc sample resistivity measured at 25 K [18].

$$\frac{\sigma_1}{\sigma(25)} = 4\frac{RX/R(25)X(25)}{[(R/R(25))^2 + (X/X(25))^2]^2};$$
$$\frac{\sigma_2}{\sigma(25)} = 2\frac{(X/X(25))^2 - (R/R(25))^2}{[(R/R(25))^2 + (X/X(25))^2]^2} \tag{3}$$

$\sigma_2/\sigma_2(0)$ is normalized to the value at T = 0, $\sigma_2(0) = \sigma_2(T = 0)$. The condition $\sigma_2 = 0$ and $\sigma_1 = \sigma(25K)$ is verified at 25 K in Eq. (3).

The temperature dependence of the conductivity σ_1 and σ_2 obtained for the underdoped

$BaFe_{1.93}Ni_{0.07}As_2$ and $BaFe_{1.925}Ni_{0.075}As_2$ -crystals previously reported in [12] are shown with two logarithmic scales in Figs. 1 and 2.

We consider carefully the behavior of the conductivity in the temperature range below 25 K. $\sigma_1/\sigma(25K)$ and $\sigma_2/\sigma_2(0)$ exhibit a first increase below T_M = 21 K and a second increase below the superconducting phase transition T_C (16 K and 13 K) for the underdoped $BaFe_{1.93}Ni_{0.07}As_2$ and $BaFe_{1.925}Ni_{0.075}As_2$ crystals respectively.

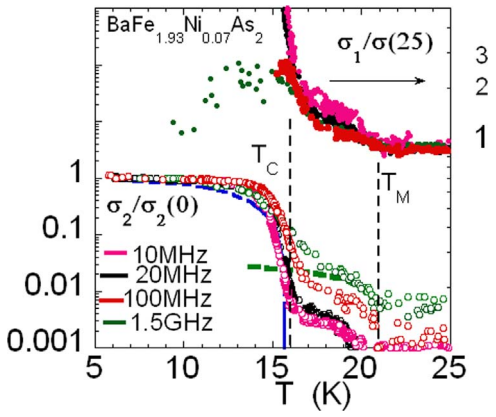

Fig. 1. (color on line) Temperature dependence of the real $\sigma_1/\sigma(25)$ (filled symbols) and imaginary $\sigma_2/\sigma_2(0)$ (open symbols) parts of the electronic conductivity, $\sigma(25)$ is the conductivity at 25 K for the underdoped $BaFe_{1.93}Ni_{0.07}As_2$ crystals. Calculated $(\sigma_2/\sigma_2(0))_{fit}$ at 1.5 GHZ (green dashed line) using Eq. (7) with $\omega\tau_{mag0} = 0.4$. Blue dashed line is calculated with $\sigma_2/\sigma_2(0) = 1\text{-}(T/16)^2$. Data taken from Fig. 4 in reference [12].

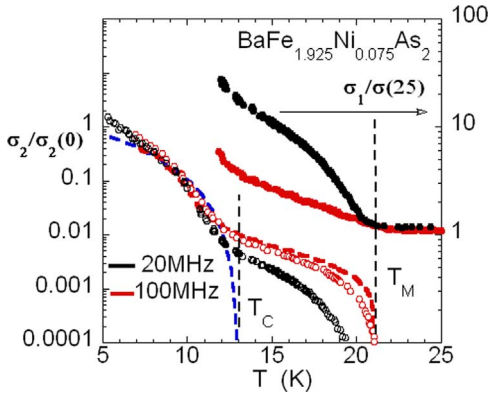

Fig. 2. (color on line) Temperature dependence of the real $\sigma_1/\sigma(25)$ (filled symbols) and imaginary $\sigma_2/\sigma_2(0)$ (open symbols) parts of the electronic conductivity, $\sigma(25)$ is the conductivity at 25 K for the underdoped $BaFe_{1.925}Ni_{0.075}As_2$ crystals data taken from reference [12]. Calculated $(\sigma_2/\sigma_2(0))_{fit}$ at 1.5 GHZ (red dashed line) using Eq. (7) with $\omega\tau_{mag0} = 0.5$. Blue dashed line is calculated with $\sigma_2/\sigma_2(0) = 1\text{-}(T/13)^2$.

Such an strange behavior of the electronic conductivity in the temperature range Tc-T_M is intriguing (Fig. 1, 2). In contrast with our previous work [12] we do not attribute this effect to a broad superconducting transition. We note that $\sigma_2/\sigma_2(0)$ increases with frequency in the temperature range T_C -T_M (Fig. 2). In contrast $\sigma_2/\sigma_2(0)$ is independent of frequency below T_C (Fig. 1). This finding suggests another possible origin. A magnetic ordering below $T_M \sim 21$ K could be responsible for such anomalous temperature behavior of σ_1 and σ_2.

A similar behavior of the conductivity has been observed in $DyNi_2B_2C$ compound which exhibits superconductivity coexisting with magnetic order [20]. We use the analysis developed in [20]. The complex permeability $\mu = \mu_0(1+j\omega\tau_{mag})$ in the ordered magnetic state below T_M is attributed to a relaxation time τ_{mag}. A complex permeability is algebraically equivalent to a Drude type conductivity

$$\sigma_1 - j\sigma_2 = (\sigma_{1cor} - j\sigma_{2cor})/(1 + j\omega\tau_{mag}) \tag{4}$$

where $\sigma_{1co\ r}$ - $j\sigma_{2co\ r}$ is the corrected conductivity and $\sigma_1 - j\sigma_2$ is the apparent conductivity.

Surface impedance is now given by

$$Z = R + jX = \sqrt{\frac{j\mu_0\omega}{\sigma_1 - j\sigma_2}} = \sqrt{\frac{j\mu_0\omega(1 + j\omega\tau_{mag})}{\sigma_{1cor} - j\sigma_{2cor}}} \tag{5}$$

The corrected conductivity is given by

$$\sigma_{1cor}/\sigma(25) = \sigma_1/\sigma(25) + [\sigma_2/\sigma(25)]\omega\tau_{mag}$$
$$\sigma_{2cor}/\sigma(25) = \sigma_2/\sigma(25) - [\sigma_1/\sigma(25)]\omega\tau_{mag} \quad (6)$$

if $\omega\tau_{mag} < 1$.

The real part of the correct conductivity σ_{1cor} takes into account of the total dissipation in the system, losses attributable to the conductivity and a small contribution from the spin dynamics. As pointed out in [20] the corrected σ_{2cor} conductivity is the measure of the superfluid density in the system and should be = 0 for T > Tc. It results that the temperature dependence of the scattering time τ_{mag} can be obtained from the temperature dependence of $\sigma_2/\sigma(25)$ in the temperature range above Tc. The experimental data points $\sigma_2/\sigma_2(0)$ are relatively well described in the temperature range between T_C and T_M by a critical scattering time

$\tau_{mag} = \tau_{mag0}(1\text{-}T/T_M)^{o0.4}$ which increases from zero to τ_{mag0}. The calculated curve

$$\left(\frac{\sigma_2}{\sigma_2(0)}\right)_{fit} = \left[\frac{\sigma_1}{\sigma(25)}/\frac{\sigma(25)}{\sigma_2(0)}\right]\omega\tau_{mag0}(1-\frac{T}{T_M})^{0.4} \quad (7)$$

is shown in Fig. 1a the dashed green curve is evaluated with $\omega\tau_{mag\ 0}$ = 0.4 at 1.5 GHz. A similar value $\omega\tau_{mag0}$ = 0.5 is found at 100 MHz with $BaFe_{1.93}Ni_{0.07}As_2$. The dashed red curve in Fig. 2 is evaluated with Eq. (7) and $\omega\tau_{mag0} \sim 1$ at 100 MHz with $BaFe_{1.925}Ni_{0.075}As_2$. Scattering time $\tau_{mag\ 0} \sim 10^{-10}$ s and 10^{-9} s is estimated at 1.5 GHz and 100 MHz respectively.

The real part of the corrected conductivity is given by the following equation

$$\sigma_{1cor}/\sigma(25) = \sigma_1/\sigma(25) + [\sigma_2/\sigma(25)]\omega\tau_{mag0}(1 - T/T_M)^{0.4} \quad (8)$$

The enhancement of the corrected σ_{1cor} below T_M results from the temperature dependent scattering time τ_{mag} increasing rapidly with decreasing temperature. The conductivity of σ_1 increases with decreasing temperature below T_C to a maximum of about 2 –10 times its normal value and this maximum decreases with increasing frequency from 20 to 1500 MHz. Such a behavior could be related to a coherence peak whose amplitude increases with decreasing frequency. The sharp increase of the σ_1 below T_C was explained by a rapid increase of the quasi particle scattering time with decreasing temperature [14,15,19,21].

The corrected σ_{2cor} data evaluated with Eq. (6) using $\omega\tau_{mag\ 0}$ = 0.4 and 0.5 at 100 and 1500 MHz respectively for $BaFe_{1.93}Ni_{0.07}As_2$ are shown in Fig. 3a. The corrected σ_{2cor} data evaluated with Eq. (6) using $\omega\tau_{mag\ 0}$ = 0.4 at 100 MHz above 12 K (red diamonds symbols) for $BaFe_{1.925}Ni_{0.075}As_2$ is shown in Fig. 3b. The corrected σ_{2cor} data shows the continuous decrease of Eq. (1) with increasing temperature from 0 to T_C and σ_{2cor} = 0 for T > T_C.

3. Elastic constant measurements

Anomalous behavior of the longitudinal elastic constant C_{33} and its correlation with superconductivity in Co and Ni doped $BaFe_2As_2$ has been studied in [10] and [13] respectively.

The measurements of the velocity and attenuation of the longitudinal C_{33} and shear C_{44} modes propagating along the c axis for the underdoped $BaFe_{1.93}Ni_{0.07}As_2$ and reported in [13] are re-examined. The standard pulse echo technique was used at 15 and 45 MHz with LiNbO3 transducers and the experimental procedure is described in [13].

A large decrease ~ 0.2% of the elastic constant C_{33} and a broad maximum in attenuation have been observed with Co optimally doped $BaFe_2As_2$ around the superconducting phase transition T_C in [10]. In contrast a narrow specific heat anomaly is observed at T_C [10]. The authors proposed that the large anomaly appearing around T_C in C_{33} can be related to inter layer properties having a magnetic origin. A large decrease in the velocity of the elastic modes C_{33} and C_{44} has been

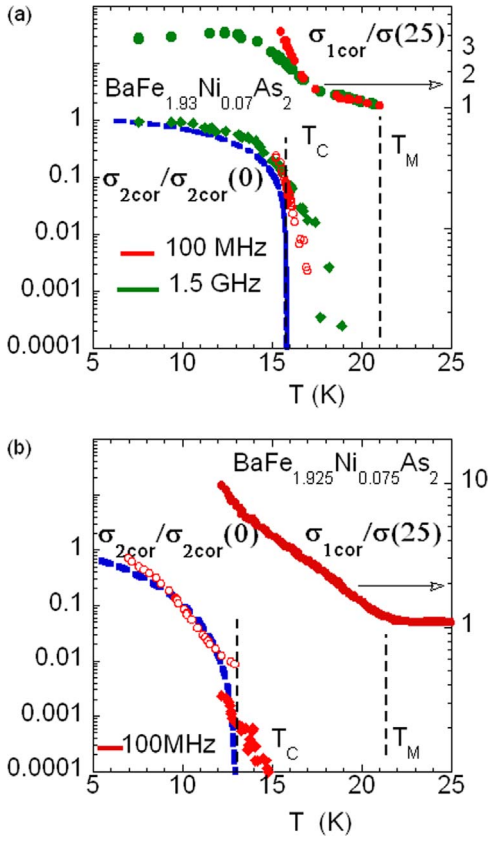

Fig. 3. (color on line) a)Temperature dependence of the real $\sigma_{1cor}/\sigma(25)$ corrected electronic conductivity at 1.5 GHz (filled green symbols) and at 100 MHz (filled red symbols) calculated with Eq. (8) with $\omega\tau_{mag0}$ = 0.4 and 0.5 respectively for the underdoped $BaFe_{1.93}Ni_{0.07}As_2$ crystals. Temperature dependence $\sigma_{2cor}/\sigma_{2cor}(0)$ at 1.5 GHZ (diamond symbols) at 100 MHz (red open symbols) deduced with Eq. (6) and $\omega\tau_{mag0}$ = 0.4 and 0.5 respectively. Blue dashed line is calculated with $\sigma_{2cor}/\sigma_{2cor}(0) = 1\text{-}(T/16)^2$. b) Temperature dependence of the real $\sigma_{1cor}/\sigma(25)$ of the corrected conductivity at 100 MHz (red filled symbols) using Eq. (8) with $\omega\tau_{mag0}$ = 1. Temperature dependence of the imaginary part $\sigma_{2cor}/\sigma_2(0)$ of the corrected conductivity for the underdoped $BaFe_{1.925}Ni_{0.075}As_2$ crystals at 100 MHz (red diamond symbols). Temperature dependence of the imaginary part $\sigma_2/\sigma_2(0)$ of the apparent conductivity at 100 MHz (red open symbols) below T_C. Blue dashed line is calculated with $1\text{-}(T/13)^2$.

observed around the superconducting phase transition with the underdoped $BaFe_{1.93}Ni_{0.07}As_2$ crystals reported in [13] and shown in Fig. 4. Each elastic constant is related to the corresponding velocity by $C = \rho V^2$, where ρ is mass density ρ = 6.5 g/cm^3, C_{33} = 70 GPa and C_{44} = 20 GPa are measured at room temperature [13].

The purely electromagnetic effects observed in the temperature range $T_C - T_M$ in the underdoped $BaFe_{1.93}Ni_{0.07}As_2$ crystals are concomitant with the decrease of the velocity of the elastic modes C_{33} and C_{44} observed in the same underdoped crystals reported in [13] and shown in Fig. 4. The appearance of a discontinuity on the velocity V_{33} of the longitudinal mode C_{33} at the superconducting transition is related by thermodynamics [22] to the jump in the specific heat ΔC_p and the uniaxial pressure dependence dT_C/dp_c along the c axis

$$\frac{\Delta C_{33}}{C_{33}} = -\frac{C_{33}\Delta C_p}{T_C V_m}\left(\frac{dT_C}{dp_c}\right)^2 \quad (9)$$

where $\Delta C_{33}/C_{33} = 2\Delta V_{33}/V_{33}$ and V_m is the volume per mol ($V_m = 4 \times 10^{-5}$ m^3/mol). We can determine a Grüneisen parameter Γ along the c axis using Eq. (8)

$$\frac{\Delta C_{33}}{C_{33}} = -\Gamma^2\frac{T_C}{C_{33}}\Delta C_p \quad \text{with} \quad \Gamma = \frac{C_{33}}{T_C}\frac{dT_C}{dp_c} \quad (10)$$

Adiabatic elastic constant are obtained in ultrasonic measurements and adiabatic dT_C/dp_c and Γ parameters are estimated with Eqs. (9)

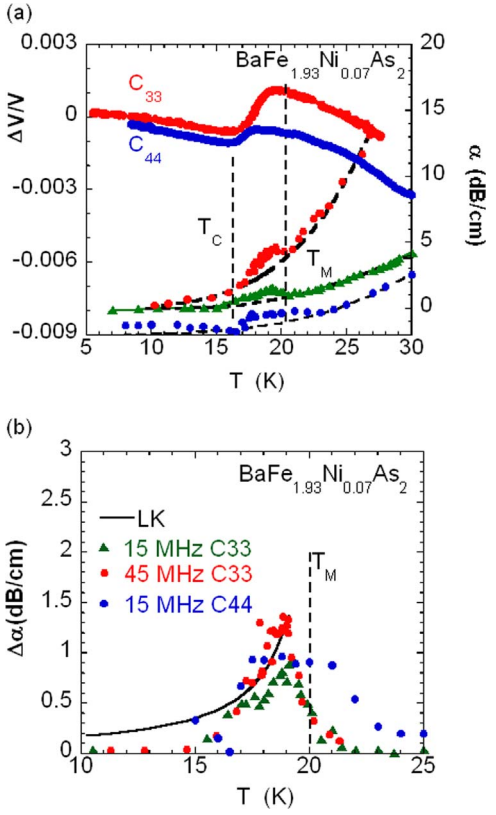

Fig. 4. (color on line) a)Relative change of the velocity of the longitudinal C_{33} (red symbols) and shear C_{44} (blue symbols) modes of underdoped $BaFe_{1.93}Ni_{0.07}As_2$. Data taken from Fig. 3 and 5 in [13]. Attenuation of the C_{33} mode measured at 15 MHz (green triangles) and 45 MHz (red circles), attenuation of the C_{44} mode measured at 15 MHz (blue circles). For clarity the points of the different modes have been shifted. The dashed lines are the background attenuation fits. b) Attenuation $\Delta\alpha = \alpha - \alpha_{background}$ of the C_{33} (green triangles 15 MHz, red circles 45 MHz) and C_{44} (blue circles 15 MHz)) modes. The black solid line LK is calculated at 45 MHz with Eq. (11) and $\tau_{LK} = 1 \times 10^{-10}(1 - T/T_M)^{-1}$.

Table 1
Superconducting phase transition T_C, elastic constant decrease $\Delta C_{33}/C_{33}$, specific jump ΔC_p, uniaxial pressure derivative dT_C/dp_c and Grüneisen parameter Γ along the c axis⊡.

	T_C (K)	$\Delta C_{33}/C_{33}$	ΔC_p (J/ (mol K))	dT_C/dp_c (K/ Gpa)	Γ
$BaFe_{1.93}Ni_{0.07}As_2$	16	0.004 [13]	0.19 [3]	14	64
$BaFe_{1.88}Ni_{0.12}As_2$	15	0.0004 [13]	0.13 [3] 0.1 [13]	5	22

and (10) and reported in Table 1. The decrease $\Delta C_{33}/C_{33} \sim 0.004$ is found in the underdoped $BaFe_{1.93}Ni_{0.07}As_2$ crystal which is comparable to that found in the optimally doped $Ba(Fe_{0.94}Co_{0.06})_2As2$ crystal [10]. Similar dT_C/dp_c and Γ parameters are found in the Ni and Co doped $BaFeAs_2$ superconductors. A smaller decrease $\Delta C_{33}/C_{33} \sim 0.0004$ is observed for the overdoped $BaFe_{1.88}Ni_{0.12}As_2$ crystals [13]. The uniaxial pressure dependence dT_C/dp_c along the c axis decreases with increasing Ni concentration in contrast with the results obtained with the Co doped $BaFeAs_2$ superconductors which are characterized by an increase of dT_C/dp_c with increasing Co concentration [10].

The appearance of a decrease around the superconducting phase transition of the velocity of the shear elastic mode C_{44} propagating along the c axis shown in Fig. 4 and previously reported in [13] is unusual. The decrease of the velocity of the mode C_{44} starts at T_M with a broad peak in the attenuation in the temperature range T_C-T_M. The specific heat measurements indicate an anomaly at T_C but not at T_M [3].

The steplike anomaly of the velocity of the C_{33} mode suggests that the coupling between the order parameter Q and the elastic strain e_3 has the form e_3Q^2 [10]. Such a quadratic coupling between a longitudinal strain and the order parameter is expected at a superconducting transition [23–25]. Magneto elastic coupling of the form $e_3Q_M^2$ with the magnetic order parameter Q_M gives a step like decrease of the longitudinal velocity at the magnetic transition [10].

It is interesting to note that the velocity of the shear elastic mode C_{44} exhibits also a steplike decrease around T_C. Such an anomaly in the shear elastic constants is unusual in conventional superconducting transition but step like decreases of several shear elastic constants has been observed in layered organic superconductors for multidimensional orders parameters and related to interlayer effects [24,25]. The orthorhombic D_{2h} symmetry group is associated with the underdoped $BaFe_{1.93}Ni_{0.07}As_2$ crystal. It results from symmetry considerations that the order parameter Q must have two contributions characterized by two orthonormal basis functions Q_1 and Q_2 in order to explain the step like decrease of the shear elastic C_{44} as discussed in [25]. Q_1 and Q_2 transform according to the irreducible representations A_{1g} and B_{3g} respectively or B_{1g} and B_{2g} respectively. This result suggests that the order parameter in underdoped $BaFe_{1.93}Ni_{0.07}As_2$ crystal is sensitive to interlayer effects and the properties of C_{44} depend of interlayer coupling.

The broad attenuation in the ordered phase below T_M can be discussed on the basis of Landau Khalatnikov relaxation mechanism [23]. The order parameter is characterized by a relaxation time τ_{LK} and the ultrasonic attenuation is expressed as a function of the angular frequency ω and τ_{LK}

$$\Delta\alpha = \frac{\Delta V}{V^2}\frac{\omega^2\tau_{LK}}{1 + (\omega\tau_{LK})^2} \quad (11)$$

Δα is maximum at a temperature T_{max} when $\omega\tau_{LK} = 1$.

Relaxation time τ_{LK} follows the critical temperature dependence $\tau_{LK} = \tau_{LK}^0(1\text{-}T/T_M)^{-1}$. The ultrasonic attenuations of the C_{33} and C_{44} modes below T_M can be described by Eq. (10) using the relaxation time $\tau_{LK} = 1 \times 10^{-10}(1\text{-}T/T_M)^{-1}$.

The anomalies in elastic constants C_{33} and C_{44} and the electrodynamic properties of the underdoped $BaFe_{1.93}Ni_{0.07}As_2$ crystal are not been quantitatively described and remain an enigma [10]. The domain structure which always appears in the pnictide crystals could give a contribution to the elastic properties. With increasing Ni or Co concentration the domain structure becomes more intertwined due to a decrease in the orthorhombic distortion [26].

4. Conclusion

The large anomalies exhibited around the superconducting phase transition by the longitudinal C_{33} and shear C_{44} modes in the underdoped $BaFe_{1.93}Ni_{0.07}As_2$ crystal are related to the unusual temperature dependence the electronic conductivity. Below $T_M = 21$ K establishment of a magnetic affect profoundly the electronic conductivity. The enhancement of the real part σ_{1cor} of the conductivity is attributed to the increase of the electron scattering time τ_{mag} when local magnetic order sets in. Such a magnetic ordering at $T_M = 21$ K has an effect on the electrodynamic properties in the superconducting state below $T_C = 16$ K.

A similar anomaly in C_{33} was observed in the optimally doped $Ba(Fe_{0.94}Co_{0.06})_2As_2$ crystal around the superconducting phase transition [10]. Such anomalies observed in the elastic longitudinal and shear modes propagating along the c axis perpendicular to the basal planes are not yet completely understood but could be due to three dimensional effects and inter layer fluctuations of magnetic origin [10].

References

[1] A.E. Böhmer, C. Meingast, C. R. Physique 17 (2012) 90–112.
[2] M. Yoshizawa, S. Simayi, Mod. Phys. Lett. B 26 (2012) 1230011.

[3] D. Gong, T. Xie, X. Lu, C. Ren, L. Shan, R. Zhang, P. Dai, Y. Yang, H. Luo, S. Li, Phys. Rev. B 93 (2016) 134520.
[4] X. Lu, D.W. Tam, C. Zhang, H. Luo, M. Weng, R. Zhang, L.W. Harriger, T. Keller, B. Keimer, L.-P. Regnault, T.A. Meir, P. Dai, Phys. Rev. B 90 (2014) 024509.
[5] X. Lu, H. Gretarson, R. Zhang, X. Liu, H. Luo, W. Tian, M. Laver, Z. Yamani, Y.-J. Kim, A.H. Nevidomskyy, Q. SI, P. Dai, Phys. Rev. Lett. 110 (2013) 257001.
[6] P. Wiecki, B. Roy, D.C. Johnston, S.L. Bud'ko, P.C. Canfield, Y. Furukawa, Phys. Rev. Let. 115 (2015) 137001.
[7] A.P. Dioguardi, J. Crocker, A.C. Shockley, C.H. Lin, K.R. Shirer, D.M. Nisson, M.M. Lawson, N. apRoberts-Warren, P.C. Canfield, S.L. Bud'ko, S. Ran, N.J. Curro, Phys. Rev. Lett. 111 (2013) 297201.
[8] R. Zhou, Z. Li, D.L. Sun, C.T. Lin, G.-Q. Zheng, Nat. Commun. 4 (2013) 2265.
[9] P. Dai, Rev. Mod. Phys. 87 (2015) 855–896.
[10] S. Simayi, K. Sakano, H. Takezawa, M. Nakamura, Y. Nakanishi, K. Kihou, M. Nakajima, C.-H. Lee, A. Ivo, H. Eisaki, S.-I. Uchida, M. Yoshizawa, J. Phys. Soc. Jpn. 82 (2013) 114604.
[11] M. Saint-Paul, C. Guttin, A. Abbassi, Z.-S. Wang, H. Luo, X. Lu, C. Ren, H.-H. Wen, K. Hasselbach, Solid State Commun. 185 (2014) 10–13.
[12] M. Saint-Paul, C. Guttin, A. Abbassi, Z.-S. Wang, H. Luo, X. Lu, C. Ren, H.-H. Wen, K. Hasselbach, Solid State Commun. 192 (2014) 47–50.
[13] M. Saint-Paul, A. Abbassi, Z.-S. Wang, H. Luo, X. Lu, C. Ren, H.-H. Wen, K. Hasselbach, Physica C 483 (2012) 207–212.
[14] A. Barannik, N.T. Cherpak, M.A. Tanatar, S. Vitusevich, V. Skresanov, P.C. Canfield, R. Prozorov, Phys. Rev. B 87 (2013) 014506.
[15] J.S. Bobowski, J.C. Baglo, J. Day, P. Dosanjh, R. Ofer, B.J. Ramshaw, R. Liang, D.A. Bonn, W.N. Hardy, H. Luo, Z.-S. Wang, L. Fang, H.-H. Wen, Phys. Rev. B 82 (2010) 094520.
[16] Y. Wu, S. Luo, X.B. Jiang, F. Zhou, L.X. Cao, Y.S. He, N.T. Cherpak, V.N. Skresanov, A. Barannik, J. Supercond. Nov. Magn. 26 (2013) 1221–1225.
[17] R. Prozorov, V.G. Kogan, Rep. Prog. Phys. 74 (2011) 1245051–12450520.
[18] Y. Chen, X. Lu, M. Wang, H. Luo, S. Li, Supercond. Sci. Tecnol. 24 (2011) 065004–065008.
[19] K. Hashimoto, T. Shibauchi, S. Kasahara, K. Ikada, S. Tonegawa, T. Kato, R. Okazaki, C.J. van der Beek, M. Konczykowski, H. Takeya, K. Hirata, T. Terashima, Y. Matsuda, Phys. Rev. Lett. 102 (2009) 207001.
[20] D.P. Choudhury, H. Srikanth, S. Sridhar, P.C. Canfield, Phys. Rev. B 58 (1998) 14490.
[21] D.A. Bonn, R. Liang, T.M. Riseman, D.J. Baar, D.C. Morgan, K. Zhuang, P. Dosanjh, T.L. Duty, A. Macfarlane, G.D. Morris, J.H. Brewer, W.N. Hardy, C. Kallin, A.J. Berlinsky, Phys. Rev. B 17 (1993) 11314–11327.
[22] L.R. Testardi, Phys. Rev. B 12 (1975) 3849–3854.
[23] B. Lüthi, M. Cardona, P. Fulde, K. von klitzin, H.J. Queisser (Eds.), Physical Acoustics in The Solid State, Springer-Verlag Berlin, 2005.
[24] B. Lüthi, S. Zherlitsyn, B. Wolf, Eur. Phys. J. B 46 (2005) 169–176.
[25] M. Dion, D. Fournier, M. Poirier, K.D. Truong, A.-M.S. Tremblay, Phys. Rev. B 80 (2009) 220511.
[26] R. Prozorov, M.A. Tanatar, N. Ni, A. Kreyssig, S. Nandi, S.L. Bud'ko, A.I. Goldman, P.C. Canfield, Phys. Rev. B 80 (2009) 174517.